scientific reports

Check for updates

OPEN

Effect of acetylcholine deficiency on neural oscillation in a brainstem-thalamus-cortex neurocomputational model related with Alzheimer's disease

Hao Yang[1], XiaoLi Yang[1]✉, SiLu Yan[1] & ZhongKui Sun[2]

Previous works imply that involving brainstem in neuropathological studies of Alzheimer's disease (AD) is of clinically significant. This work constructs a comprehensive neural mass model for cholinergic neuropathogenesis that involves brainstem, thalamus and cortex, wherein how acetylcholine deficiency in AD affects neural oscillation of the model output is systematically explored from the perspective of neurocomputation. By decreasing synapse connectivity parameters in direct cholinergic pathway from brainstem to thalamus or in indirect glutamatergic synapse pathway from cortex to brainstem to mimic the pathological condition of reduced acetylcholine release in patients with AD, the property of neural oscillation in this model is numerically investigated by means of power spectrum in frequency domain and amplitude distribution in time domain. Simulated results demonstrate that decreasing synapse connectivity whether in the direct cholinergic pathway or in the indirect glutamatergic synapse pathway can alter the neural oscillation significantly in three aspects: it induces an obvious decrease of dominant frequency; it leads to a degraded rhythmic activity in the alpha frequency band as well as an enhanced rhythmic activity in the theta frequency band; it results in reduced oscillation amplitude of the model output. These results are agreement with the characteristic of electrophysiological EEG measurement recorded in AD, especially support the hypothesis that cholinergic deficiency is a promising pathophysiological origin of EEG slowing in AD. Our analysis indicates that targeting the cholinergic system may have potential prospects in early diagnosis and treatment of AD.

As we all know, the brain is the largest and most complex structure of the central nervous system, which is closely related to consciousness, memory and other activities[1]. Damage to some brain regions would cause neurological or psychiatric disorders such as epilepsy, Alzheimer's disease (AD) and autism. AD is a neurodegenerative disease of the nervous system in the elderly. Only when irreversible damage occurs to the brain can AD be detected, so it poses a very serious threat to the health of AD patients[2].

The cholinergic hypothesis indicates that the cholinergic system in patients with AD is abnormal. Cholinergic action is important to maintain attention and memory[3,4]. Relevant studies have found that there are massive loss of cholinergic neurons and decrease of acetylcholine release in the brain of AD patients[5–8]. In addition, the brainstem contains a large number of cholinergic neurons projecting to the thalamus[9–11] which can maintain the cortical excitability during wakefulness and rapid eye movement sleep[12,13]. In order examine that the brainstem nuclei are vulnerable to AD-related pathological changes, Parvizi et al.[14] have performed a study of thioflavin S-stained serial sections in the entire brainstem, in which they have found that the physiological markers of AD, senile plaques and neurofibrillary tangles, are respectively existed in superior colliculus and cholinergic nucleus in 32 AD patients, whereas no changes are seen in the brainstem of 26 normal subjects. The above findings imply that AD may relate with the degeneration of cholinergic neurons in the brainstem, especially the cholinergic pathway from the brainstem to the thalamus may be important to understand the pathogenesis of AD.

[1]School of Mathematics and Statistics, Shaanxi Normal University, Xi'an 710062, People's Republic of China. [2]School of Mathematics and Statistics, Northwestern Polytechnical University, Xi'an 710072, People's Republic of China. ✉email: yangxiaoli@snnu.edu.cn

There have been considerable laboratory researches, such as neuroimaging, neurochemistry and gene mapping, to identify potential AD marker for early preventative treatments of AD. Electroencephalographic (EEG), for its sensitivity to brain pathology, relative non-invasiveness and ease of measurement, has become a popular neurophysiological technique to study AD. Some typical EEG changes including the reduced dominant frequency (also called peak frequency)[15–17] and the slowing of EEG signals in AD patients[17–21] have been revealed. Moreover, in a review of EEG dynamics in AD patients, Jeong[20] has stated that the pathophysiological origin for EEG slowing in AD may be largely due to acetylcholine deficiency. This statement is also supported by EEG experiment in healthy subjects using scopolamine (a kind of muscarinic receptor antagonist), in which there appears an increase in the delta and theta power, and a decrease in the alpha and beta power after administrating scopolamine[22].

In order to better understand the mechanism behind the activity of brain neurons, many neurocomputational models have been developed, roughly categorized as detailed model and neural mass model[23–29]. The detailed model is too computationally complicated to analyze the whole behavior in a relatively large brain region. For the neural mass model, each cell population represents a neuronal ensemble of mesoscopic scale, which is lumped together and supposed to share same membrane potential. One of the first neural mass model was proposed first by Wilson and Cowan[30,31] based on the interaction of one excitatory population and one inhibitory population. Then, Silva et al.[32] have established an alpha rhythm model in the thalamus to mimic the generation of alpha rhythm. Subsequently, Jansen and Rit[33] have changed the impulse response function to construct a neural mass model in a single cortical column. Wendling et al.[34] have included the population of GABA interneurons with fast synaptic kinetics into the Jason and Rit's model, where they produced realistic multichannel epileptiform EEG signal in the hippocampus. Nowadays, the neural mass model proposed by Jansen and Rit has been frequently extended to coupled neural mass models to simulate the complexity of EEG dynamics in large cortical region[28,29,34–36]. In addition, Bhattacharya et al. have proposed a thalamus-cortex-thalamus (TCT) neural mass model consisting of a thalamic module and a cortical module, in which the synaptic connectivity related to the aberration of the alpha rhythm in the brain resulting from AD is discussed[37]. Recently, Li et al. have improved the TCT model by incorporating the disinhibition property between different inhibitory interneurons in the cortical region and introducing the full relay function of thalamus to the cortical region[26], which is helpful to understand the neuronal correlates of slowing of the alpha rhythm induced by AD.

Although some neural mass models comprising cortical column, thalamus or hippocampus have been successfully exploited to simulate some specific aspects of brain rhythms and the abnormal brain activity during disease, they have not been used to analyze the underlying brain dynamics in the brainstem associated with AD. In addition, as indicted in the previous work[9,12,14], in brainstem there are different nuclei involving in many functions, such as controlling homeostasis and emotions, modulating the cognitive functions of cerebral cortex, thus understanding its involvement in AD is clinically significant. Nevertheless, the status of most subcortical structures including the brainstem remains poorly understood during AD compared with the majority of neuropathological studies of AD from the cortical aspect. Some manifestations of AD (e.g. behavioral, affective, and cognitive abnormality) may be interpreted from the perspective of dysfunction in subcortical structure of brainstem[14]. Thus, with a purpose to mimic the EEG dynamics observed in patients of AD, this work extends the neural mass model to build a comprehensive model in the interactive brain structures of brainstem, thalamus and cortex (i.e., a BTC model), in which how abnormal acetylcholine release affects the neural oscillations of the model output is explored.

The following is organized as follows. Firstly, model presentations including how to construct the BTC model and its related model parameters are illustrated in "An enhanced neural mass model: brainstem thalamus cortexmodel" Section . Then the effect of reduced synapse connectivity resulting from AD on the neural oscillation in this BTC model is systematically studied by numerical simulations in "Main result" Section. Finally, a brief summary of this work is present.

An enhanced neural mass model: brainstem-thalamus-cortex model. As described in the Introduction, in addition to the thalamic and cortical aspects, the involvement of brainstem is also of significance to AD[9,12,14]. In this section, based on the neural mass models in cortical and thalamic regions[26,37], a comprehensive neural mass model in the interactive brain regions of brainstem, thalamus and cortex (BTC) is firstly constructed by newly adding two brainstem neuron populations-superior colliculus and the pedunculopontine nucleus. As shown in Fig. 1, this BTC model is made of a brainstem module, a thalamus module and a cortex module. There are two populations of superior colliculus (SC) and pedunculopontine nucleus (PNN) in the brainstem module, where the PNN population produces excitatory synapse on the SC population, as implied by the work[11]. The thalamus module is modeled by three populations of thalamic relay nucleus (TRC), inhibitory interneurons (IN) and thalamic reticular nucleus (TRN)[26,32,37–39]. The TRC population receives inhibitory inputs from the IN and TRN populations via intrinsic synapse pathway, whereas the TRN population receives excitatory inputs from the TRC population. The IN and TRN populations also receive inhibitory inputs from themselves, respectively. The module of cortex is built upon four populations of pyramidal neurons (PY), excitatory interneurons (eIN), fast inhibitory interneurons (fIN) and slow inhibitory interneurons (sIN)[26,28,29,34,37]. Within this module, the PY population sends excitatory outputs to the sIN and fIN populations, in turn, both the sIN and fIN populations send inhibitory outputs to the PY population. There are reciprocal excitatory outputs between the PY and eIN populations, and there are reciprocal inhibitory outputs between the sIN and fIN populations. For the interconnections between the three modules, as indicated in the studies[9–11,40,41], there are cholinergic and glutamatergic synapse pathway from the brainstem area to the thalamus area. The thalamic nuclei are modulated by an ascending cholinergic projection from the brainstem via cholinergic neurotransmitter. Depending on different muscarinic receptor subtypes, the PNN population sends exhibitory outputs to the TRC population by means of M1 and M3 receptor subtypes[42], also it sends inhibitory outputs to the IN and TRN populations by means of

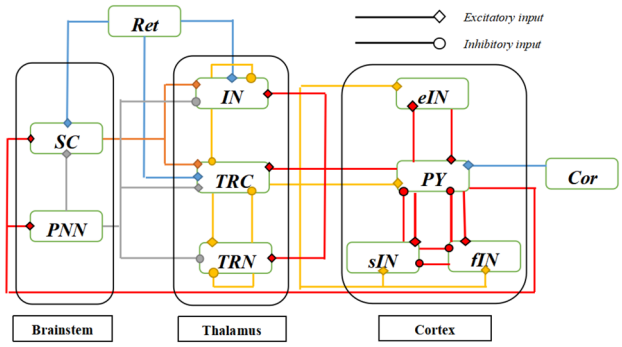

Figure 1. The layout for module structure and synaptic connectivity in the BTC model. The BTC model comprises of three formations: brainstem module, thalamus module and cortex module. In the brainstem module there are two populations of superior colliculus (SC) and pedunculopontine nucleus (PNN). In the thalamus module there are thalamic relay nucleus (TRC), inhibitory interneurons (IN) and thalamic reticular nucleus (TRN). In the cortex module there are pyramidal neurons(PY), excitatory interneurons (eIN), fast inhibitory interneurons (fIN) and slow inhibitory interneurons (sIN). Ret and Cor denote external visual inputs and adjacent cortical inputs respectively. Diamond represents excitatory inputs and circle represents inhibitory inputs.

M2 receptor subtype[9–11,43]. Meanwhile, the SC population in the brainstem sends excitatory outputs to the TRC and IN populations via glutamatergic neurotransmitter[40,41]. The synaptic interconnections between the thalamus and the cortex modules conform to the classical results as presented in the literatures[26,36,37], i.e., all the populations of TRC, IN and TRN in the thalamus region receive excitatory inputs from the PY population, on the same time, the TRC population sends excitatory outputs to all the populations of PY, eIN, fIN and sIN in the cortical region. In addition to the ascending synapses from the brainstem to the thalamus and cortex, there is important descending synapse pathway from the cortex to the brainstem in the central nervous system[44,45]. Here, the PY population in the cortex module sends excitatory outputs to the SC and PNN populations in the brainstem module. Other extrinsic sources to the BTC model come from the retinal and nearby cortical formations, i.e., the retinal population sends excitatory outputs to the IN, TRC and SC populations, and the PY population receives excitatory afferent from nearby cortical regions[26,28,29,36,37].

For convenience, neuron populations in this model are denoted by different lowercase letters $s, d, i, t, n, h, p, f, l, r$ and c, which represent populations SC, PNN, IN, TRC, TRN, eIN, PY, fIN, sIN, Ret, Cor, respectively. According to the technique of neural mass model, the kinetic equations governing each population are obtained by performing two mathematical operations. One is that the average membrane potential V_a in each population a (here $a = s, d, i, t, n, h, p, f, l, r, c$) receiving from all afferent neuronal populations is changed into an average density of spikes φ_a, which is usually simulated by the following sigmoidal function:

$$\varphi_a = S(V_a) = \frac{2e_0}{1 + e^{\sigma(V_0 - V_a)}} \tag{1}$$

$$V_a = \sum_b C_{abe} x_b - \sum_d C_{adi} x_d \tag{2}$$

where C_{abe} represents excitatory synaptic connection parameter between postsynaptic neuron population a and presynaptic neuron population b, and C_{adi} represents inhibitory synaptic connection parameter between postsynaptic neuron population a and presynaptic neuron population d. x_b and x_d are postsynaptic potential (PSP) respectively generated by population b and d. e_0 determines the maximum firing rate, V_0 is the firing threshold, σ controls the steepness of this sigmoid function.Note that the average density of spikes for neuron population Ret is simulated by Gaussian white noise $P_1(t)$ with mean μ_1 and variance ε_1. The average density of spikes for neuron population Cor is simulated by Gaussian white noise $P_2(t)$ with mean μ_2 and variance ε_2.The other mathematical operation is that a second linear transform function of pulse response converts the presynaptic average spikes density φ_a into the postsynaptic membrane potential x_a, which is as follows:

$$\tau_a^2 x_a'' = A_a \tau_a \varphi_a - 2\tau_a x_a' - x_a \tag{3}$$

where A_a is the synaptic strength determining the maximum amplitude of PSP, and τ_a represents the time constant of PSP. Please refer to the detailed mathematical equations governing all the 11 neuron populations in this BTC model in the Supplementary Material section.

The connectivity parameters of afferent to the brainstem and thalamus modules are according to the previous physiological data[46–50]. In detail, based on the electron microscopic observances on the connectivity patterns of two main cell types in the lateral geniculate nucleus of the cat, Erisir et al.[46] have revealed that distribution of synapse is different between relay cells and interneurons present in this nucleus. The relative distribution of terminal types contacting relay cells is $14.6 \pm 0.6\%$ retinal (RLP) terminals, $29.6 \pm 1.6\%$ inhibitory (F) terminals, and 55.8

$\pm$ 1.7% cortex and brainstem terminals. Whereas, the analysis of the total synaptic inputs onto the interneurons indicates that interneurons receive 37.8 $\pm$ 1.0% of all synapses from retinal terminals, 26.8 $\pm$ 1.5% from inhibitory terminals, and 35.4 $\pm$ 1.8% from cortex and brainstem terminals. Moreover, in geniculate A-laminae the relay cells and the interneurons receive 85.8 $\pm$ 0.6% and 14.2 $\pm$ 0.6% of all synaptic terminals, respectively, i.e., the synaptic terminals contacting the relay cells is about 6 times of that contacting the interneurons. Erisir et al.[47] have further found that the relative number of cortical inputs and brainstem inputs to the lateral geniculate nucleus is of the same order, each of whose terminals constitutes roughly one-half. As for the TRN afferent axons, Jones have reported that almost 70% synaptic inputs to the reticular nucleus in the somatosensory sector of the rat is attributed to corticothalamic terminals, 20–25% is attributed to thalamocortical collateral synapses, 15–20% is attributed to $GABA_{ergic}$ synapses and a quite small number of inputs is from the brainstem[48]. Another study has reported that the synaptic proportions from corticothalamic, thalamocortical and $GABA_{ergic}$ synapse are respectively 60–65%, 20% and 15%[49]. The study of Haith et al. has showed that SC and the dorsal lateral geniculate nucleus (including TRC and IN) respectively account for 15% and 85% of the retinal ganglion cells (output cells of retinal)[50]. On the basis of the above studies[46–50] the connectivity parameters relative with the brainstem and thalamus modules are determined. On the same time, the connectivity parameters afferent to the cortex module are sourced from the works[26,28,33,34,51]. The detailed values for all the connectivity parameters are described in Table 1 in the Supplementary Material section. In addition, the synaptic strength A_a, time constant τ_a, as well as other basic parameters (e_0, V_0, σ, μ_1, ε_1, μ_2, ε_2) in the BTC model are referenced from previous works[26,33,37], which are outlined in Table 2 in the Supplementary Material section.

Main result

As described in the Introduction, previous reports about reduced ACh release, loss of cholinergic neurons and decreased ChAT activity in AD patients have indicated that acetylcholine release is abnormal in AD patients[5–8]. In brainstem there are a large number of cholinergic neurons projecting to thalamus, moreover, the brainstem nuclei such as superior colliculus and cholinergic nucleus are susceptible to AD[9–11]. This implies that AD is associated with degeneration of the direct cholinergic pathway from brainstem to thalamus. In addition, the neuroimaging technique has shown that loss of functional/structural connectivity in cortical areas have been related to cortical atrophy in AD from graph theoretical studies[52,53]. This property of cortical atrophy may influence the descending synapse projection from cortex to brainstem[44,45], which in turn could weaken the cholinergic pathway from brainstem to thalamus indirectly. Thus, this study simulates the pathological condition of reduced acetylcholine release in AD by decreasing the synapse connectivity parameters in the direct cholinergic pathway from brainstem to thalamus (i.e., C_{tde} from PNN to TRC, C_{idi} from PNN to IN, C_{ndi} from PNN to TRN) and the indirect glutamatergic synapse pathway from cortex to brainstem(i.e.,C_{dpe} from PY to PNN). How the abnormal acetylcholine release affects neural oscillation in this BTC model is systematically explored by means of power spectrum and amplitude distribution.

In the following, the second-order differential equations governing the BTC model are numerically solved by Euler method in an environment of MATLAB 2019a. The total simulation time is 120 s with a time resolution of 1/256 s. The model output corresponds to the summated postsynaptic potential V_t in the TRC population. For each output vector, an epoch is extracted in the interval of [20, 120] s to ensure that all the transients are discarded. The epoch of output is then bandpass filtered by a Butterworth filter of order 10 with a lower and upper cut-off frequencies of 0.5 and 50 Hz, respectively. The detailed analysis of power spectrum and oscillation amplitude are further carried out based on the filtered output.

Decreasing the excitatory cholinergic connectivity from PNN to TRC. The level of cholinergic neurotransmitter from the PNN population in the brainstem module to the TRC population in the thalamus module is determined by the excitatory synapse connectivity parameter C_{tde}. In this section, through decreasing the strength of C_{tde} to mimic the degeneration of acetylcholine release in patients with AD, neural oscillation of this BTC model is firstly characterized by means of power spectrum analysis in frequency-domain. Based on the filtered output of V_t, the power spectrum density of the BTC model is computed using the Welch technique with a Hamming window. Quantitative analysis of power spectrum is performed by characterizing dominant frequency and measuring relative power in specific frequency bands. Dominant frequency is a frequency at which the power spectrum density reaches its peak. The relative power of alpha band (8-13 Hz) or theta band (4-8 Hz) is calculated by averaging the relative power spectrum density within the corresponding frequency band.

The dominant frequency of the model output is illustrated in Fig. 2a when the connectivity parameter C_{tde} is varied in the rage of[60, 100]. On the whole, the dominant frequency shows a downward trend from 9.25 to 6.25 upon decreasing C_{tde} from 100 to 60: it is initially within the alpha band, then the dominant frequency decreases steadily until C_{tde} is decreased to a critical value of about 80, at which the dominant frequency transits from the alpha band to the theta band, afterwards it decreases continually within the theta band as C_{tde} is further decreased. That is to say, the smaller the excitatory cholinergic synapse connectivity parameter C_{tde}, the lower the dominant frequency. This phenomenon is further vividly confirmed by some individual plots of power spectrum density. Figure 2b depicts the detailed power spectrum density when the connectivity parameter C_{tde} is successively chosen as 100, 82, 70 and 60. Clearly, peaks of the power spectrum density in the upper two panels of Fig. 2b are concentrated at the alpha frequency band of 9.25 and 8.5 respectively when C_{tde} is more than 80, whereas peaks in the lower two panels of Fig. 2b are centered at the theta frequency band of 7 and 6 respectively when C_{tde} is less than 80. These interesting results indicate that acetylcholine deficiency, a biomarker for AD, can induce an obvious decrease of dominant frequency, which is consistent with the electrophysiological experiment results that the dominant/peak frequency of EEG is significantly lower in early stage of AD than that in control subjects[15–17].

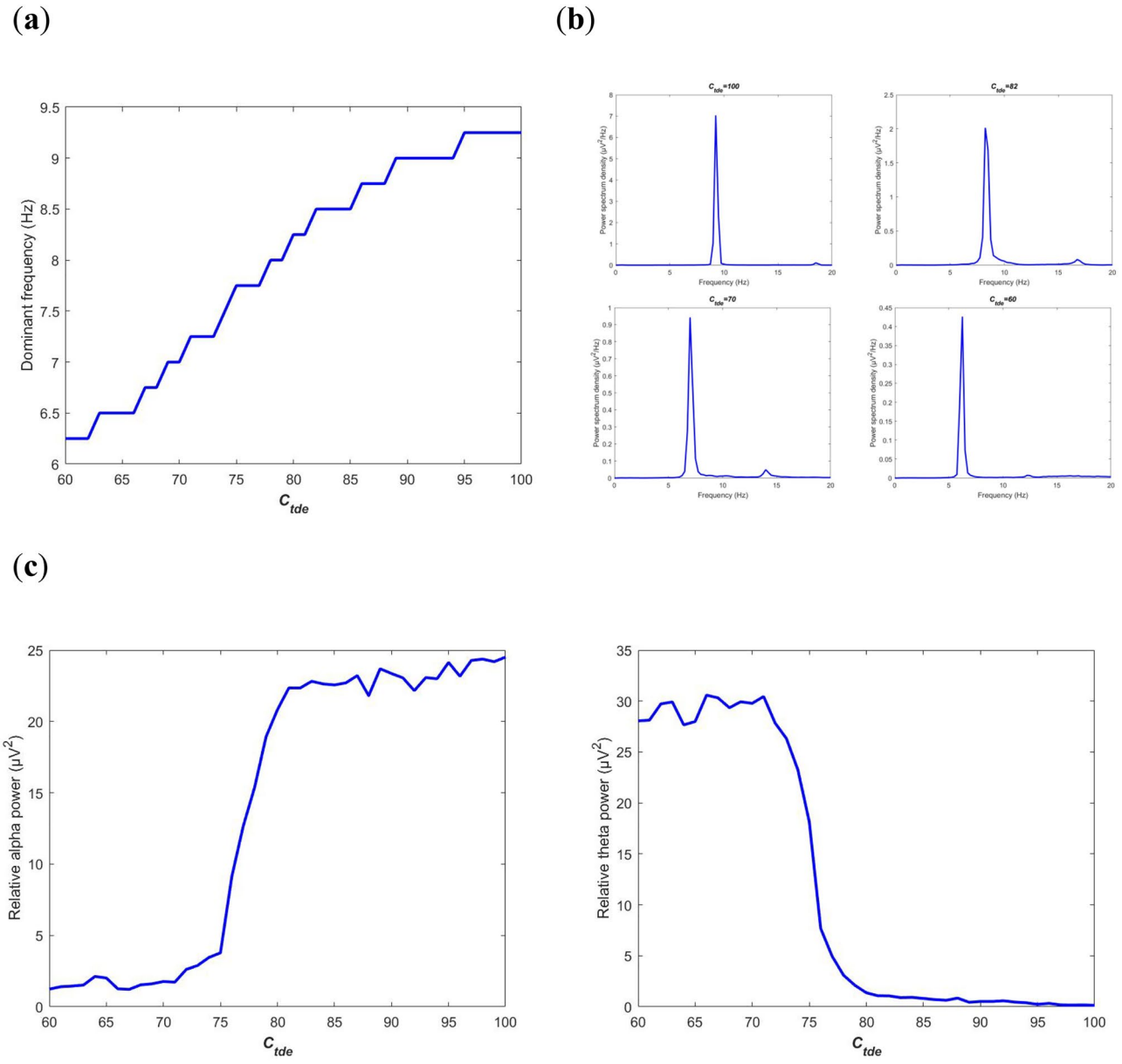

Figure 2. Power spectrum analysis of the BTC model output V_t in frequency-domain when the excitatory synapse connectivity parameter C_{tde} from PNN to TRC is varied in the range of [60, 100]. (**a**) Dependence of the dominant frequency of the model output on C_{tde}. (**b**) Individual plots of power spectrum density when C_{tde} takes some different values of 100, 82, 70 and 60. (**c**) The evolution of relative power in specific frequency bands: alpha frequency band (left panel) and theta frequency band (right panel).

Furthermore, the power spectrum analysis of relative power in specific frequency bands is carried out. The relative power within the alpha band and within the theta band is respectively illustrated in Fig. 2c when the excitatory synapse connectivity parameter C_{tde} is in the range of[60, 100]. One can observe that upon decreasing C_{tde} from 100, the relative alpha band power decreases slightly until C_{tde} arrives at the critical value of about 80, then it falls sharply till $C_{tde} \approx 73$, after which the relative power in alpha band does not decrease anymore and basically tends to be stable. Interestingly, the evolution of the relative theta band power is opposite to that of the relative alpha band power. In detail, upon decreasing C_{tde} from 100 to 60, the relative power in theta band is just a little increased till C_{tde} reaches the critical value of about 80, then it grows swiftly until $C_{tde} \approx 73$, after that the relative theta band power fluctuates slightly with the further decrease of C_{tde}. This phenomenon accords with the traditional experiment EEG measurements that there is a decrease in the alpha band activity and an increase in theta band activity in patients with AD[17–21], in particular, it supports the hypothesis that cholinergic deficiency is a promising pathophysiological origin of the EEG slowing in AD[20,22].

Secondly, neural oscillation of this BTC model is investigated by means of oscillation amplitude in time-domain. When decreasing the excitatory synapse connectivity parameter C_{tde} from 100 to 60, the model output, i.e., the summated postsynaptic potential V_t in the TRC population, is illustrated in Fig. 3a for each value of C_{tde}.

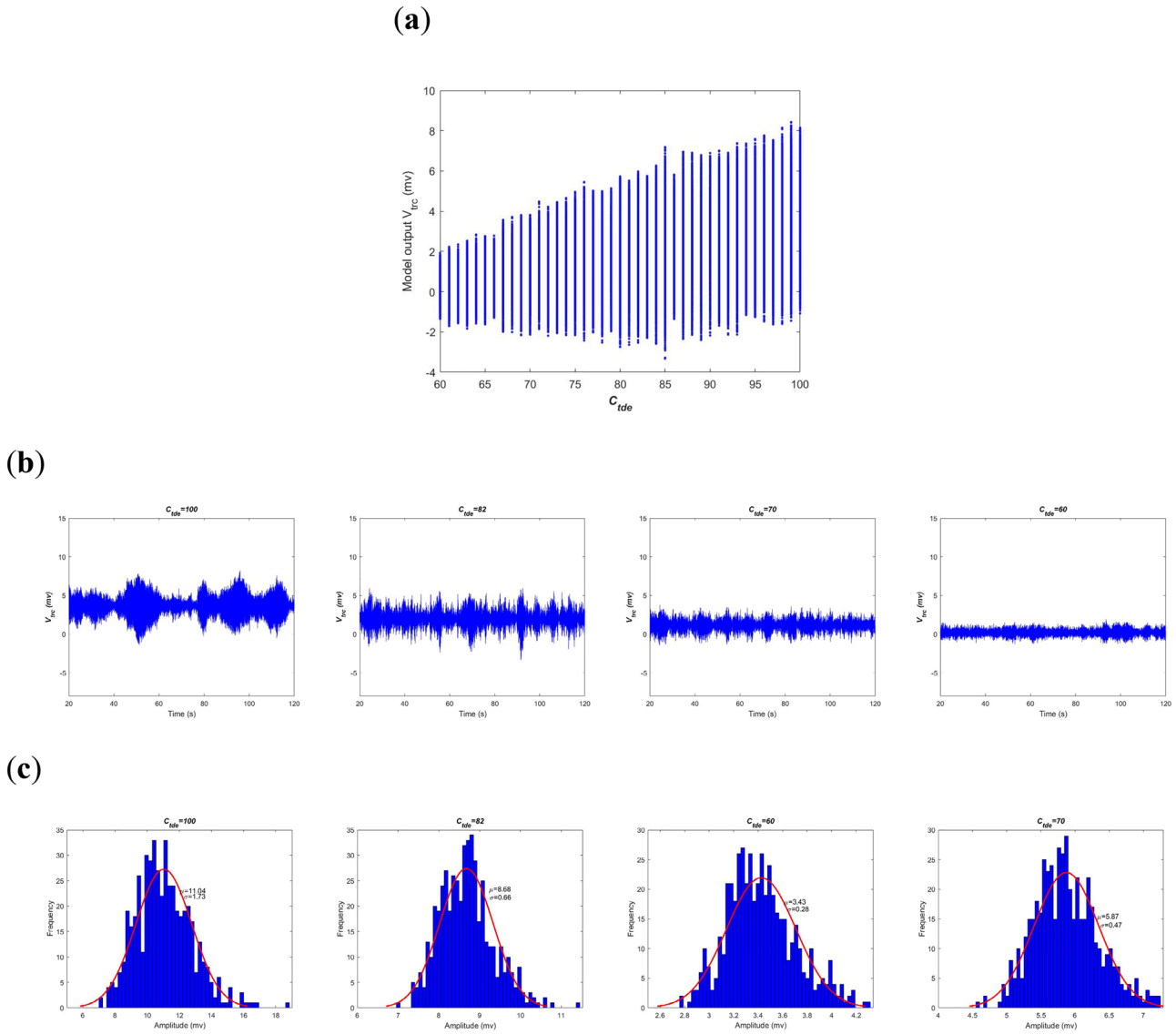

Figure 3. Amplitude analysis of the BTC model output V_t in time-domain when the excitatory synapse connectivity parameter C_{tde} from PNN to TRC is varied in the range of [60, 100]. (**a**) The model output of the summated postsynaptic potential V_t for each C_{tde}. (**b**) Diagram of the summated postsynaptic potential V_t during [20, 120]s when C_{tde} takes some different values of 100, 82, 70 and 60. (**c**) Amplitude distribution of V_t based on 500 realizations of postsynaptic potential when C_{tde} takes some different values of 100, 82, 70 and 60.

The longitudinal coordinate (y-axis) of this figure is the summated postsynaptic potential V_t during [20, 120]s of simulations. Obviously, as a whole the oscillation amplitude of V_t is getting smaller upon decreasing the synapse connectivity parameter C_{tde}. To visualize this result, the detailed postsynaptic potential V_t for some typical synaptic strengths such as $C_{tde} = 100$, 82, 70 and 60 is also depicted in Fig. 3b. one can qualitatively observe that the oscillation amplitude of V_t is gradually reduced with the decrease of connectivity parameter. Especially, for the two former ones the BTC model produces rhythmic oscillation of potential analogous to alpha-rhythm (with the dominant frequency within alpha band as shown in Fig. 2b), i.e., they exhibit waxes and wanes in amplitude just like a form of spindle[32]. There is no obvious qualitative change in dynamics from the perspective of time series. As the synapse connectivity C_{tde} is less than the critical value of 80, the output of BTC model in the latter two panels presents rhythmic oscillation of the theta frequency band (with the dominant frequency within the theta band as shown in Fig. 2b) with relative small amplitude compared to the former two cases. Due to the influence of the noise, statistical and uncertainty analysis is performed in order to avoid the randomness. Furthermore, as displayed in the Fig. 3c the statistical property of oscillatory potential is characterized by amplitude distribution based on 500 realizations of postsynaptic potential. Here the histogram of oscillation amplitude is fitted by normal density function with estimated parameters of mean and variance. As can be seen in the Fig. 3c, the estimated mean of oscillation amplitude is 11.04, 8.68, 5.87 and 3.43 when the connectivity parameter C_{tde} is successively taken as 100, 82, 70 and 60. This result further quantitatively confirms that the reduced oscillation amplitude of the model output results from the decreased excitatory synapse connectivity parameter C_{tde}, i.e., a hallmark of deficit cholinergic synapse pathway from the PNN population to the TRC population.

Decreasing the inhibitory cholinergic connectivity from PNN to IN and TRN. In addition to the above excitatory cholinergic pathway from PNN to TRC via M1 and M3 muscarinic receptor subtypes, there are also two inhibitory cholinergic pathways from PNN to IN and TRN via M2 muscarinic receptor subtype, whose synaptic connection are determined by C_{idi} and C_{ndi}, respectively. In this section, the physiological feature of acetylcholine deficiency in AD patients is reflected by reducing C_{idi} or C_{ndi}. Under such environment, the neural oscillation in the BTC model is investigated by means of power spectrum in frequency domain and amplitude distribution in time domain.

Firstly, neural oscillation of this BTC model is discussed on the basis of power spectrum analysis. The variation of dominant frequency of the model output V_t with the decrease of inhibitory cholinergic synaptic strength is delineated in Fig. 4a and b. One can see that whether decreasing the synapse connectivity parameter C_{idi} (from PNN to IN) or C_{ndi} (from PNN to TRN), they can always lead to a decrease of dominant frequency. To be specific, when C_{idi} (or C_{ndi}) is decreased from 18 (or 10) to a critical value of about 5 (or 2), the dominant frequency gradually drops within the alpha band, then it steps into the theta band and continually drops within theta band. To illustrate the above result more detail, some power spectrum density curves are exhibited for different synaptic connectivity parameter values. In Fig. 4c, C_{idi} is taken as 10, 6, 3 and 1 from left to right. Clearly, when C_{idi} is greater than 5, the frequency corresponding to the maximum of power spectrum density is respectively at 9.25 and 8.25, whereas when C_{idi} is less than 5, the frequency corresponding to the maximum of power spectrum density is respectively at 7 and 6. That is to say, the dominant frequency for the left two figures and the right two figures is within the alpha band and theta band respectively. In Fig. 4d, C_{ndi} is taken as 7, 3, 1.5 and 0.5 from left to right. Obviously, when C_{ndi} is larger than 2, the dominant frequency in the left two panels is at the alpha frequency band of 9.25 and 8.5 respectively, while the dominant frequency in the right two panels is at the theta frequency band of 7.5 and 7.25 respectively when C_{ndi} is smaller than 2. In addition, the relative power of the model output is calculated with the change of inhibitory cholinergic synapse connectivity C_{idi} and C_{ndi} in Fig. 4e and f. From the two panels, we can observe that upon decreasing synapse connectivity the relative theta band power (denoted by red curves with circles) increases mildly until C_{idi} (or C_{ndi}) reaches the critical value of about 5 (or 2), then it increases sharply with the further decrease of synapse connectivity. Interestingly, the relative alpha band power (denoted by blue curves with diamonds) decreases slowly till C_{idi} (or C_{ndi}) reaches the critical value of about 5 (or 2), after that it decreases swiftly with a further reduction of synapse connectivity.

In a word, the reduction of inhibitory cholinergic synaptic strength from the brainstem to the thalamus can change the rhythm of neural oscillation in the BTC model significantly. It can induce not only a diminished dominant frequency but also a slowing of rhythmic content, i.e., a decreased alpha band activity and an increased theta band activity. These simulated phenomena resulting from acetylcholine deficiency agree with the EEG characteristics observed in the electrophysiological experiments of AD patients, i.e., the major effect of AD on EEG is slowing of EEG[18–22] along with the degraded peak frequency[15–17].

Secondly, the neural oscillation of the BTC model is explored in time domain by analyzing oscillation amplitude of model output. Figure 5a and b depict the variation of the summated postsynaptic potential V_t during [20, 120]s as the inhibitory cholinergic synapse connectivity is diminished. These two figures indicate that the oscillation amplitude is degraded as a whole upon diminishing the connectivity parameter C_{idi} or C_{ndi}, though this downward trend is not very smooth. In order to confirm this phenomenon, the detailed amplitude distribution at some synaptic strengths is further displayed in Fig. 5c and d according to the statistical property of 500 realizations of postsynaptic potential V_t. From the fitted normal density function of oscillation amplitude, the Fig. 5c reveals that the estimated mean of oscillation amplitude is successively 9.58, 8.66, 6.92 and 5.41 when $C_{idi} = 10$, 6, 3 and 1. On the same time, the Fig. 5d reveals that the estimated mean of oscillation amplitude decreases from 9.83 to 8.82, then to 7.76, and finally to 6.89 when C_{ndi} decreases from 7 to 3, then to 1.5, and finally to 0.5. These results imply that decrease of inhibitory cholinergic synapse connectivity from brainstem to thalamus resulting from acetylcholine deficit can indeed bring about a decrease in oscillation amplitude of the model output.

Decreasing the excitatory glutamatergic connectivity from PY to PNN. As illustrated by the schematic of BTC model in **Fig. 1**, the release of acetylcholine from brainstem to thalamus is indirectly modulated by glutamatergic synapse pathway from cortex to brainstem. The synapse loss caused by cortical atrophy in AD may destroy the descending synapse projection from cortex to brainstem[44,45]. In this section, decreasing the glutamatergic synapse connectivity C_{dpe} from PY in cortex to PNN in brainstem to mimic indirect acetylcholine deficiency, neural oscillation in this BTC model is discussed using power spectrum analysis and oscillation amplitude.

Firstly, the property of neural oscillation is characterized by the dominant frequency and the relative power in frequency domain. The evolution of dominant frequency of the model output V_t during the decrease of C_{dpe} is depicted in Fig. 6a. Clearly, as C_{dpe} is diminished from 78 to 38, the dominant frequency initially falls within the alpha frequency band until C_{dpe} arrives at a critical value of 45, and then the dominant frequency continues to fall within the theta frequency band with a further decrease of C_{dpe}. Individual curves of power spectrum density at some synaptic connectivity are further given in Fig. 6b to confirm the above phenomenon. As shown in the upper two panels ($C_{dpe} = 65$, 48), the peak value of power spectrum density is obtained at about 9.25 and 8.5, i.e., the dominant frequency is located within the alpha frequency band when the synaptic connectivity is large than the critical value of 45. Nevertheless, as displayed in the lower two panels ($C_{dpe} = 41$, 38), the dominant frequency is respectively 7 and 6.5, which indicates the peak of power spectrum density is located within theta frequency band when the synaptic connectivity is smaller than the critical value of 45. Furthermore, the variation of relative power along with the synaptic connectivity C_{dpe} is displayed in Fig. 6c. Upon decreasing C_{dpe} from 78, the relative alpha band power in the left panel fluctuates slightly until C_{dpe} reaches a certain value of 45, then it falls sharply till $C_{dpe} \approx 38$. Interestingly, an opposite phenomenon occurs for the evolution of the

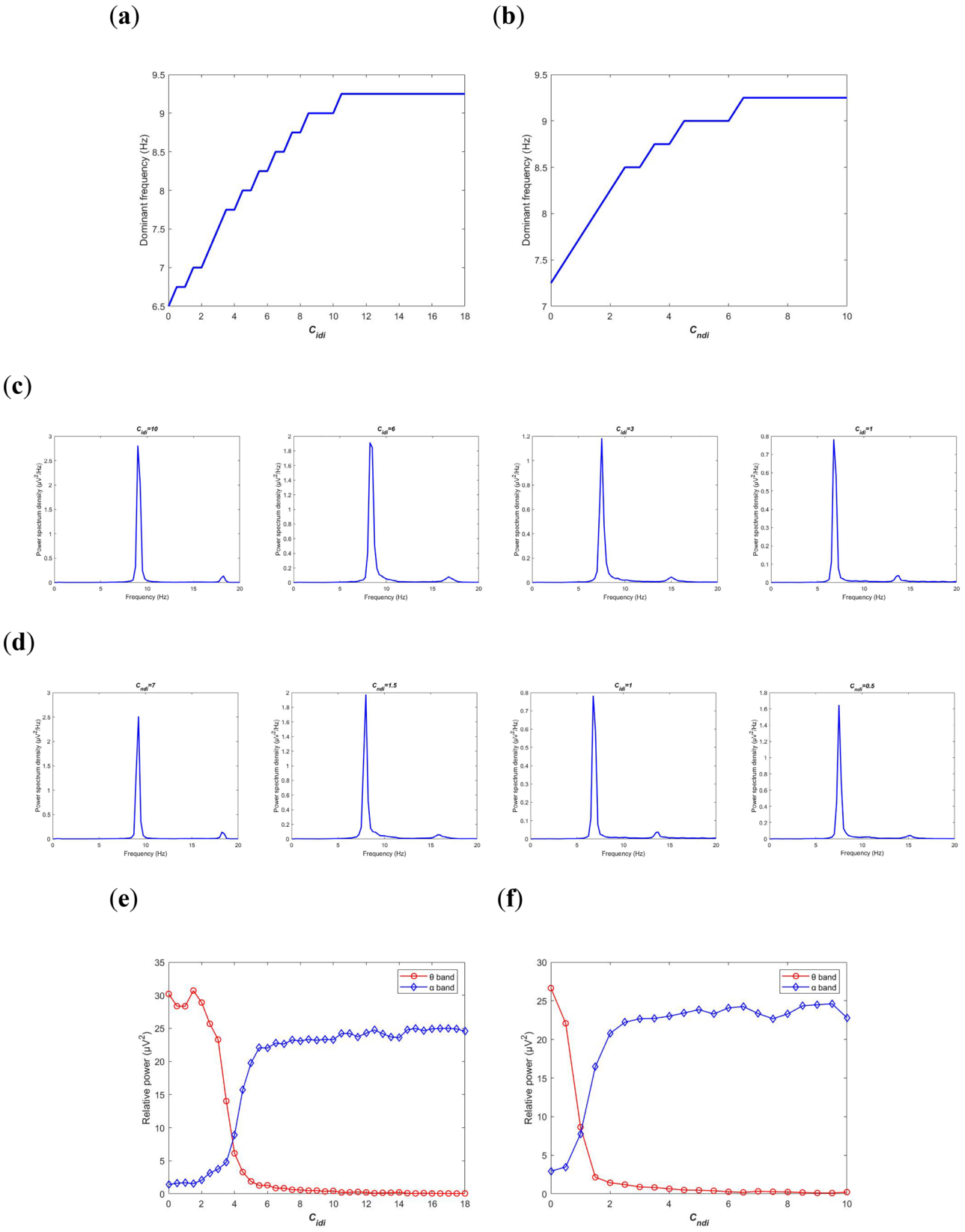

Figure 4. Power spectrum analysis of the BTC model output V_t in frequency domain with decreasing of inhibitory synapse connectivity parameters C_{idi} from PNN to IN and C_{ndi} from PNN to TRN. Dependence of the dominant frequency of the model output on C_{idi} (**a**) and C_{ndi} (**b**). The individual plots of power spectrum density when C_{idi} (**c**) and C_{ndi} (**d**) take different values. The evolution of relative power in alpha and theta frequency bands during the reduction of C_{idi} (**e**) and C_{ndi} (**f**).

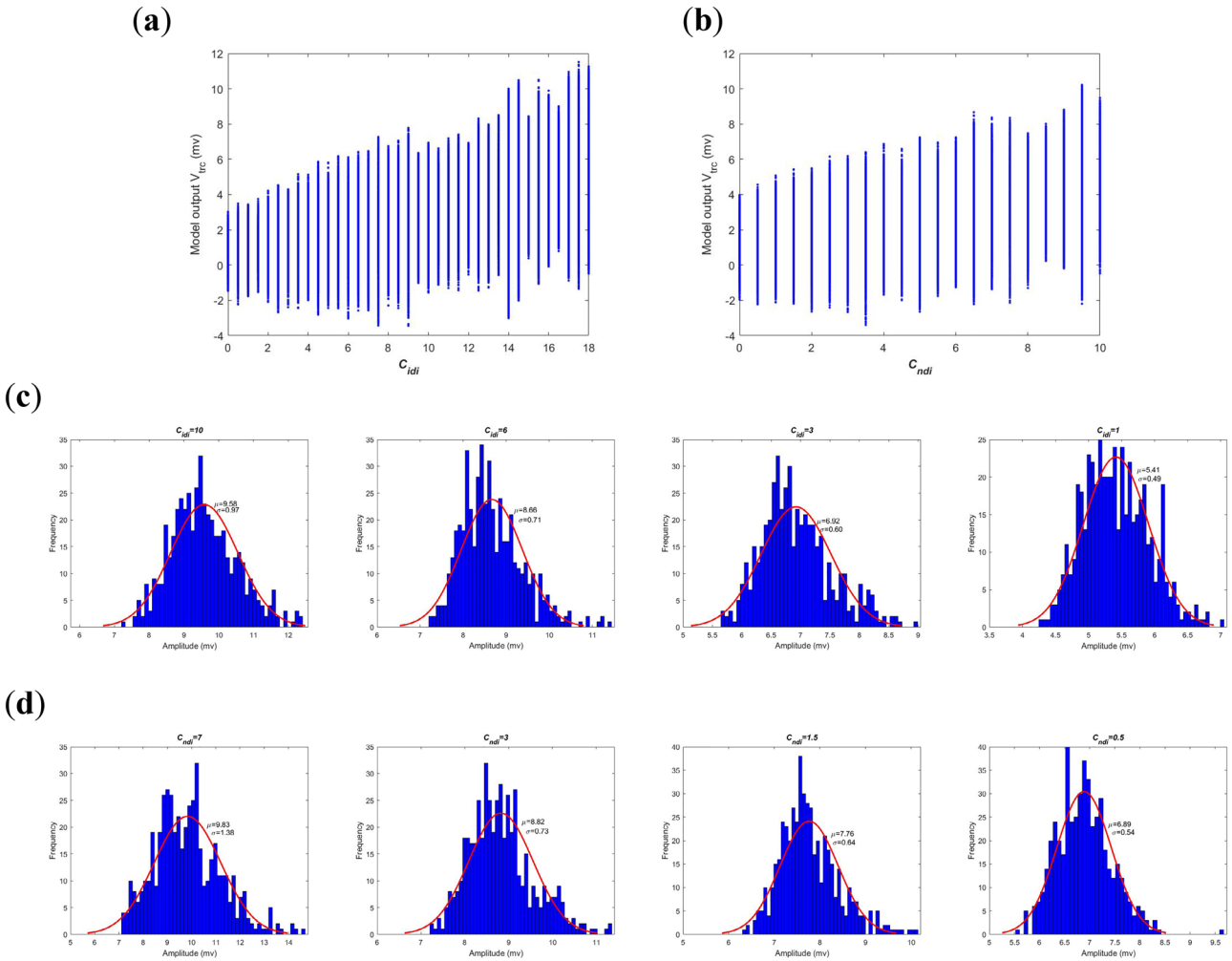

Figure 5. Amplitude analysis of the BTC model output V_t in time domain with decreasing of inhibitory synapse connectivity parameters C_{idi} from PNN to IN and C_{ndi} from PNN to TRN. The model output of the summated postsynaptic potential V_t for each C_{idi} (**a**) and C_{ndi} (**b**). Amplitude distribution of V_t based on 500 simulation results for different C_{idi} (**c**) and C_{ndi} (**d**).

relative theta band power in the right panel, i.e., the relative power within theta band rises slightly until C_{dpe} arrives at the certain value of 45, then it booms quickly till $C_{dpe} \approx 38$. As we expected, the rhythmic property of neural oscillation in this BTC model resulting from glutamatergic synapse deficit is similar with that what happened in the case of direct acetylcholine deficiency, i.e., the diminished dominant frequency, the degraded alpha band activity together with enhanced theta band activity, which is consistent with the EEG characteristic obtained from clinical trials of AD patients[15,17,20,22].

Secondly, neural oscillation of model output in the BTC model is studied by means of oscillation amplitude in time domain. Figure 7a depicts the summated postsynaptic potential V_t of model output during[20, 120] s of simulations for every connectivity parameter C_{dpe} ranged in[38, 78]. Intuitively, as C_{dpe} is decreased from 78 to 38 the oscillation amplitude of V_t slowly descends as a whole except for few connectivity parameter at which the oscillation amplitude is suddenly enlarged. In addition, this result is visualized by some individual postsynaptic potential V_t at different synaptic strength such as $C_{dpe} = 38$, 41, 48, and 65. Combined with the dominant frequency shown in Fig. 6a, the left two panels in Fig. 7b reveal that the model output has an visible alpha rhythmic content with the amplitude waxing and waning when the synapse connectivity is greater than the critical value of 45. Whereas, in the right two panels of Fig. 7b, there appears an obvious theta rhythmic content in the postsynaptic potential with relatively small oscillation amplitude when the synapse connectivity is less than the critical value of 45. Furthermore, the corresponding amplitude distribution of 500 realizations of postsynaptic potential is illustrated in Fig. 7c. One can observe that the estimated mean of oscillation amplitude is in turn 9.63, 8.96, 6.57 and 4.83 on the basis of the fitted normal density function of oscillation amplitude. This quantitative result once again confirms that the decreased oscillation amplitude of model output is due to the damaged glutamatergic synapse connectivity C_{dpe} from PY to PNN, i.e., an indirect acetylcholine synapse pathway from cortex to brainstem.

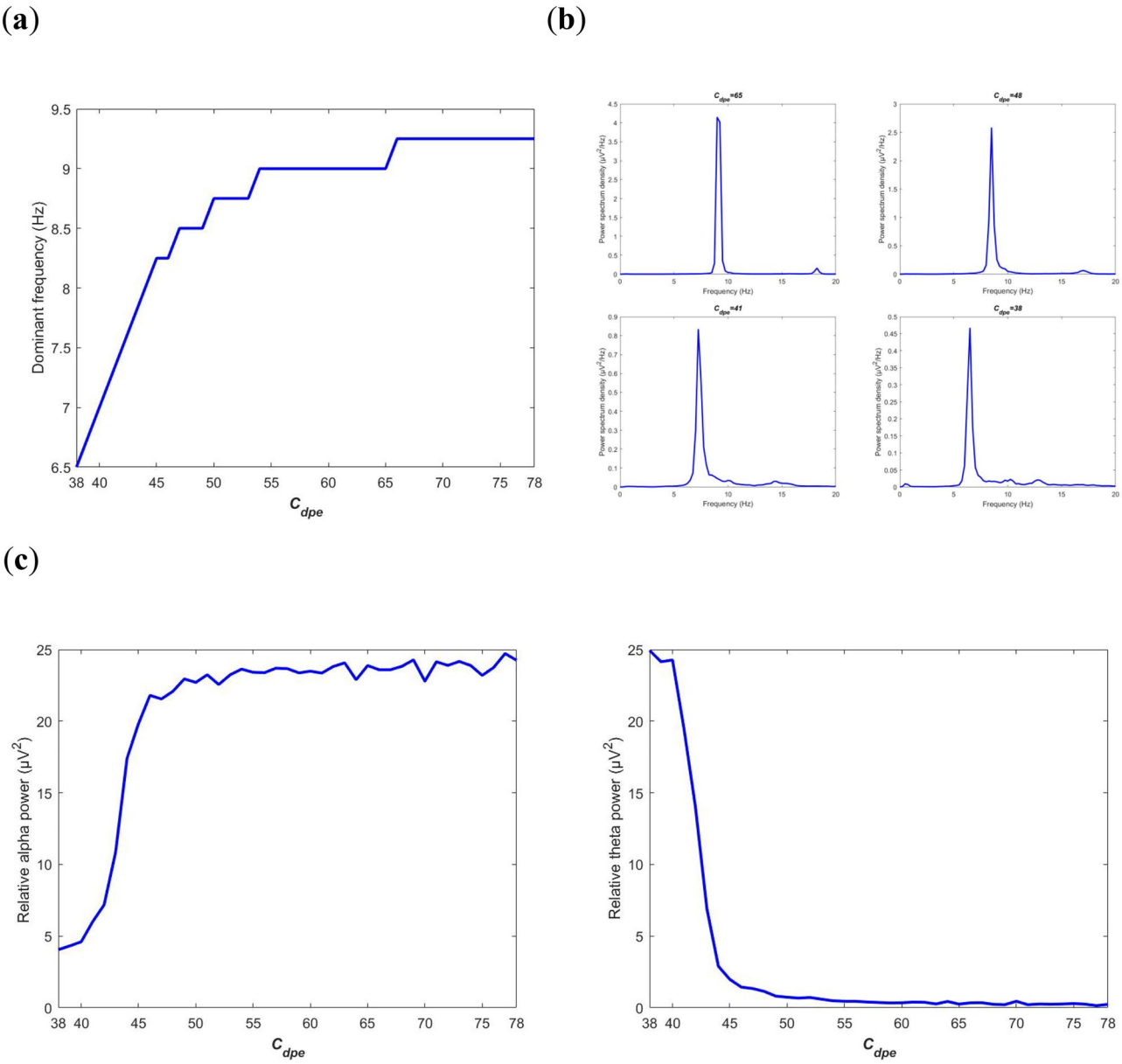

Figure 6. Power spectrum analysis of the BTC model output V_t in frequency-domain when the excitatory synapse connectivity parameter C_{dpe} from PY to PNN is varied in the range of[38,78]. (**a**) Dependence of the dominant frequency of the model output on C_{dpe}. (**b**) The power spectrum density when C_{dpe} takes some different values of 65, 48, 41 and 38. (**c**) The evolution of relative power in specific bands: alpha band (left panel) and theta band (right panel).

Conclusion and discussion

This work establishes a comprehensive neural mass model in the interactive brain structures of brainstem, thalamus and cortex. It takes destroying cholinergic synapse pathway as a surrogate for the abnormal cholinergic system in patients with AD. By monitoring synapse connectivity strength in direct cholinergic pathway from brainstem to thalamus and indirect glutamatergic synapse pathway from cortex to brainstem, we are able to simulate some property of neural oscillation in this model under an environment of acetylcholine deficiency from the standpoint of neurocomputation. By analyzing power spectrum of the model output in frequency domain, the results reveal that upon diminishing synapse connectivity strength in a certain range the dominant frequency initially decreases within alpha frequency band and then steps into theta frequency band, which is consistent with the electrophysiological experiment results that the dominant/peak frequency of EEG is significantly lower in early stage of AD than that in control subjects[15–17]. Meanwhile, the neural oscillation presents a slowing rhythmic content with a degraded alpha band relative power and an enhanced theta band relative power, which accords with the traditional experiment EEG measurements that there is a decrease in the alpha band activity and an increase in the theta band activity in patients with AD[17–21]. In particular, it supports the hypothesis that cholinergic deficiency is a promising pathophysiological origin of the EEG slowing in AD[20,22]. What's more, amplitude

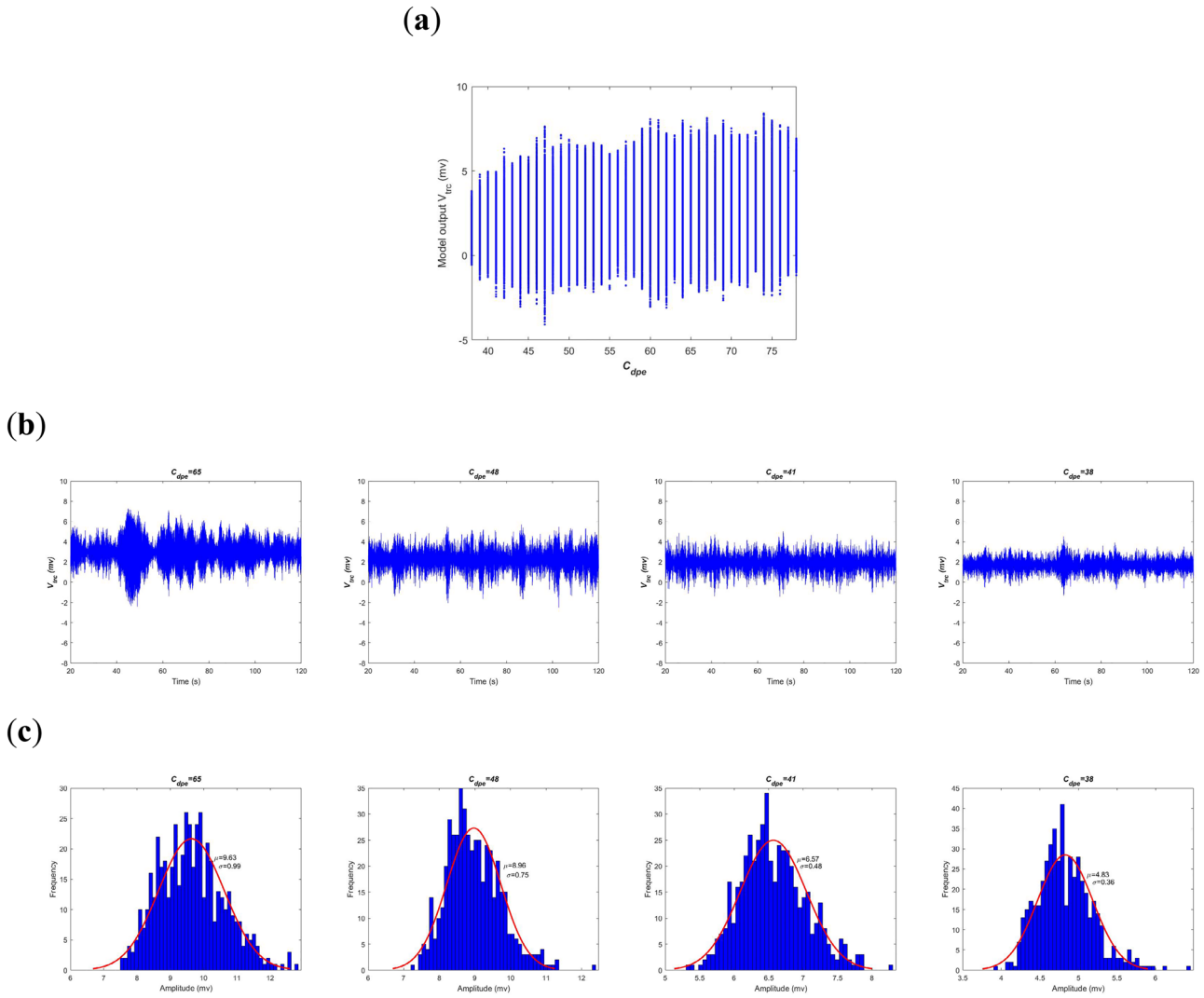

Figure 7. Amplitude analysis of the BTC model output V_t in time domain when the excitatory synapse connectivity parameter C_{dpe} from PY to PNN is varied in the range of[38,78]. (**a**) The model output of the summated postsynaptic potential V_t for each C_{dpe}. (**b**) The summated postsynaptic potential V_t during[20, 120] s when C_{dpe} takes some values of 38, 41, 48, and 65. (**c**) Amplitude distribution of V_t based on 500 simulation results when C_{dpe} takes some values of 38, 41, 48, and 65.

distribution of the neural oscillation in time domain suggests that the oscillation amplitude is overall diminished with the reduction of synapse connectivity. We expect these findings could have important implications on better understanding cholinergic pathogenesis and expounding potential feature for AD.

At last, we point out that this work, by reducing the synaptic connection parameters in cholinergic direct pathway from brainstem to thalamus or indirect glutamatergic synapse pathway from cortex to brainstem, mainly focus on the effect of acetylcholine deficiency on brain neuron activity in patients with AD. As known that there could be neuron loss and brain atrophy in cortical region in AD patients[44,45], which would induce unfavorable synapse information processing. Thus, reducing the synaptic connection parameters relative to cortical region can also simulate the pathological state of AD. Through further simulation, we find that when synapse connectivity parameter decreases from PY to TRC, the change of the dominant frequency and the oscillation amplitude is similar with what reported in this work, i. e. there is an obvious decrease of dominant frequency, a degraded rhythmic activity in the alpha frequency band as well as an enhanced rhythmic activity in the theta frequency band, and the reduced oscillation amplitude of the model output. For the limited space, we do not list them in detail.

Data availability

All data generated or analyzed during this study are included in this published article.

Received: 12 May 2022; Accepted: 26 August 2022
Published online: 02 September 2022

References

1. Zatorre, R. J., Fields, R. D. & Johansen-Berg, H. Plasticity in gray and white: Neuroimaging changes in brain structure during learning. *Nat. Neurosci.* **15**(4), 528–536 (2012).
2. Geula, C. Abnormalities of neural circuitry in Alzheimer's disease: Hippocampus and cortical cholinergic innervation. *Neurology* **51**(Suppl 1), S18–S29 (1998).
3. Hasselmo, M. E. The role of acetylcholine in learning and memory. *Curr. Opin. Neurobiol.* **16**, 710–715 (2006).
4. Sarter, M., Hasselmo, M. E., Bruno, J. P. & Givens, B. Unraveling the attentional functions of cortical cholinergic inputs: Interactions between signal-driven and cognitive modulation of signal detection. *Brain Res. Rev.* **48**, 98–111 (2005).
5. Auld, D. S., Kornecook, T. J., Bastianetto, S. & Quirion, R. Alzheimer's disease and the basal forebrain cholinergic system: Relations to beta-amyloid peptides, cognition, and treatment strategies. *Prog. Neurobiol.* **68**, 209–245 (2002).
6. Nilsson, L., Nordberg, A., Hardy, J., Wester, P. & Winblad, B. Physostigmine restores 3H-acetylcholine efflux from Alzheimer brain slices to normal level. *J. Neural Transm.* **67**, 275–285 (1986).
7. Lopez, O. L. *et al.* Severity of cognitive impairment and the clinical diagnosis of AD with Lewy bodies. *Neurology* **54**, 1780–1787 (2000).
8. Oda, Y. Choline acetyltransferase: the structure, distribution and pathologic changes in the central nervous system. *Pathol. Int.* **49**, 921–937 (1999).
9. McCormick, D. A. & Pape, H. C. Acetylcholine inhibits identified interneurons in the cat lateral geniculate nucleus. *Nature* **334**, 246–248 (1988).
10. Mesulam, M. M. Cholinergic pathways and the ascending reticular activating system of the human brain. *Ann. NY. Acad. Sci.* **757**, 169–179 (1995).
11. Billet, S., Cant, N. B. & Hall, W. C. Cholinergic projections to the visual thalamus and superior colliculus. *Brain Res.* **847**, 121–123 (1999).
12. Koyama, Y., Jodo, E. & Kayama, Y. Sensory responsiveness of "Broad-spike" neurons in the laterodorsal tegmental nucleus, locus coeruleus and dorsal raphe of awake rats: Implications for cholinergic and monoaminergic neuron-specific responses. *Neuroscience* **63**, 1021–1031 (1994).
13. Brown, R. E., Basheer, R., Mckenna, J. T., Strecker, R. E. & McCarley, R. W. Control of sleep and wakefulness. *Physiol. Rev.* **92**, 1087–1187 (2012).
14. Parvizi, J., Hoesen, G. W. V. & Damasio, A. The selective vulnerability of brainstem nuclei to Alzheimer's disease. *Ann. Neurol.* **49**, 53–66 (2001).
15. Prinz, P. N. & Vitiell, M. V. Dominant occipital (alpha) rhythm frequency in early stage Alzheimer's disease and depression. *Electroencephalogr. Clin. Neurophysiol.* **73**, 427–432 (1989).
16. Penttilä, M., Partanen, J. V., Soininen, H. & Riekkinen, P. J. Quantitative analysis of occipital EEG in different stages of Alzheimer's disease. *Electroencephalogr. Clin. Neurophysiol.* **60**, 1–6 (1985).
17. Moretti, D. V. *et al.* Individual analysis of EEG frequency and band power in mild Alzheimer's disease. *Clin. Neurophysiol.* **115**, 299–308 (2004).
18. Dauwels, J., Vialatte, F. & Cichocki, A. Diagnosis of Alzheimer's disease from EEG signals: Where are we standing. *Curr. Alzheimer. Res.* **7**, 487–505 (2010).
19. Coben, L. A., Danziger, W. & Storandt, M. A longitudinal EEG study of mild senile dementia of Alzheimer type: Changes at 1 year and at 2.5 years. *J. Electroencephalogr. Clin. Neurophysiol.* **60**, 1–6 (1985).
20. Jeong, J. EEG dynamics in patients with Alzheimer's disease. *Neurophysiology* **115**, 1490–1505 (2004).
21. Besthorn, C. Discrimination of Alzheimer's disease and normal aging by EEG data. *J. Electroencephalogr. Clin. Neurophysiol.* **103**, 241–248 (1997).
22. Ebert, U., Crossmann, M., Oertel, R., Gramatte, T. & Kirch, T. Pharmacokinetic-pharmacodynamic modeling of the electroencephalogram effects of scopolamine in healthy volunteers. *J. Clin. Pharmacol.* **41**, 51–60 (2001).
23. Jiang, P. H., Yang, X. L. & Sun, Z. K. Dynamics analysis of the hippocampal neuronal model subjected to cholinergic action related with Alzheimer's disease. *Cogn. Neurodyn.* **14**(1), 483 (2020).
24. Hassan, M. *et al.* Computational modeling and biomarker studies of pharmacological treatment of Alzheimer's disease (Review). *Mol. Med. Rep.* **18**, 639–655 (2018).
25. Breakspear, M. Dynamic models of large-scale brain activity. *Nat. Neurosci.* **20**, 340–352 (2017).
26. Li, X. Y., Yang, X. L. & Sun, Z. K. Alpha rhythm slowing in a modified thalamo-cortico-thalamic model related with Alzheimer's disease. *PLoS ONE* **15**, e0229950 (2020).
27. David, O. Neural mass models. *Brain Map.* **1**, 563–569 (2015).
28. Zavaglia, M., Astolfi, L., Babiloni, F. & Ursino, M. A neural mass model for the simulation of cortical activity estimated from high resolution EEG during cognitive or motor tasks. *J. Neurosci. Methods* **157**, 317–329 (2006).
29. Ursino, M., Cona, F. & Zavaglia, M. The generation of rhythms within a cortical region: Analysis of a neural mass model. *J. Neuroimage* **52**, 1080–1094 (2010).
30. Wilson, H. R. & Cowan, J. D. Excitatory and inhibitory interaction in localized populations of model neurons. *Biophys. J.* **12**, 1–24 (1972).
31. Wilson, H. R. & Cowan, J. D. A mathematical theory of the functional dynamics of cortical and thalamic nervous tissue. *Kybernetik* **13**, 55–80 (1973).
32. Silva, F. H. L. D., Hoeks, A., Smits, H. & Zetterberg, L. H. Model of brain rhythmic activity The alpha-rhythm of the thalamus. *Kybernetik* **15**, 27–37 (1974).
33. Jansen, B. H. & Rit, V. G. Electroencephalogram and visual evoked potential generation in a mathematical model of coupled cortical columns. *Biol. Cybern.* **73**, 357–366 (1995).
34. Wendling, F., Bartolomei, F., Bellanger, J. J. & Chauvel, P. Epileptic fast activity can be explained by a model of impaired GABAergic dendritic inhibition. *Eur. J. Neurosci.* **15**, 1499–1508 (2002).
35. Deco, G., Jirsa, V. K., Robinson, P. A., Breakspear, M. & Firstonk, K. The dynamic brain: From spiking neurons to neural masses and cortical fields. *PLoS Comput. Biol.* **4**, e1000092 (2008).
36. Spiegler, A., Kiebel, S. J., Atay, F. M. & Knösche, T. R. Bifurcation analysis of neural mass models: Impact of extrinsic inputs and dendritic time constants. *Neuroimage* **52**, 1041–1058 (2010).
37. Bhattacharya, B. S., Coyle, D. & Maguire, L. P. A thalamo-cortico-thalamic neural mass model to study alpha rhythms in Alzheimer's disease. *Neural. Netw.* **24**, 631–645 (2011).
38. Guillery, R. W. & Sherman, S. M. Thalamic relay functions and their role in corticocortical communication: Generalizations from the visual system. *Neuron* **33**, 163–175 (2002).
39. McCormick, D. A. & Bal, T. Sleep and arousal: Thalamocortical mechanisms. *Annu. Rev. Neurosci.* **20**, 185–215 (1997).
40. Kolmac, C. I. & Mitrofanis, J. Patterns of brainstem projection to the thalamic reticular nucleus. *J. Comp. Neurol.* **396**, 531–543 (1998).
41. Jeon, C. J., Gurski, M. R. & Mize, R. R. Glutamate containing neurons in the cat superior colliculus revealed by immunocytochemistry. *Visual Neurosci.* **14**, 387–393 (1997).

42. Beatty, J. A., Sylwestrak, E. L. & Cox, C. L. Two distinct populations of projection neurons in the rat lateral parafascicular thalamic nucleus and their cholinergic responsiveness. *Neuroscience* **162**, 155–173 (2009).
43. Plummer, K. L., Manning, K. A., Levey, A. I., Ress, H. D. & Uhlkich, D. J. Muscarinic receptor subtypes in the lateral geniculate nucleus: A light and electron microscopic analysis. *J. Comp. Neurol.* **404**, 408–425 (1999).
44. Matsumura, M. *et al.* Organization of somatic motor inputs from the frontal lobe to the pedunculopontine tegmental nucleus in the macaque monkey. *Neuroscience* **98**, 97–110 (2000).
45. Wallace, M. T., Meredith, M. A. & Stein, B. E. Converging influences from visual, auditory, and somatosensory cortices onto output neurons of the superior colliculus. *J. Neurophysiol.* **69**, 1797–1809 (1993).
46. Erisir, A., Horn, S. C. V. & Sherman, S. M. Distribution of synapses in the lateral geniculate nucleus of the cat: Differences between laminae A and A1 and between relay cells and interneurons. *J. Comp. Neurol.* **390**, 247–255 (1998).
47. Erisir, A., Horn, S. C. V. & Sherman, S. M. Relative numbers of cortical and brainstem inputs to the lateral geniculatenucleus. *Proc. Natl. Acad. Sci. U. S. A.* **94**, 1517–1520 (1997).
48. Jones, E. G. Thalamic circuitry and thalamocortical synchrony. *Philos. Trans. R. Soc. B-Biol. Sci.* **357**, 1659–1673 (2002).
49. Liu, X. B. & Jones, E. G. Predominance of corticothalamic synaptic inputs to thalamic reticular nucleus neurons in the rat. *J. Comp. Neurol.* **414**, 67–79 (1999).
50. Haith, G. L. Modeling Activity-Dependent Development in theRetinogeniculate Projection. https://dl.acm.org/doi/book/10.5555/927417 (Stanford University, 1998).
51. Sotero, R. C., Barreto, N. G. T., Medina, Y. I., Carbonell, F. & Jimenez, J. C. Realistically coupled neural mass models can generate EEG rhythms. *Neural Comput.* **19**, 478–512 (2007).
52. Braak, H. & Braak, E. Neuropathological stageing of Alzheimer-related changes. *Acta. Neuropathol.* **82**, 239–259 (1991).
53. Seeley, W. W., Crawford, R. K., Zhou, J., Miller, B. C. & Greicius, M. D. Neurodegenerative diseases target large-scale human brain networks. *Neuron* **62**, 42–52 (2009).

Acknowledgements

This work is partially supported by the National Natural Science Foundation of China (Grant No. 11972217).

Author contributions

H.Y. and X.Y. contributed to the conception of this work, designed research, analyzed data and wrote the main manuscript text. S.Y. and Z.S. performed the analysis and proposed constructive advice. All authors reviewed the manuscript.

Competing interests

The authors declare no competing interests.

Additional information

Supplementary Information The online version contains supplementary material available at https://doi.org/10.1038/s41598-022-19304-3.

Correspondence and requests for materials should be addressed to X.Y.

Reprints and permissions information is available at www.nature.com/reprints.

Publisher's note Springer Nature remains neutral with regard to jurisdictional claims in published maps and institutional affiliations.